doi:10.1016/j.jmb.2011.07.019 J. Mol. Biol. (2011) 412, 204–211

Contents lists available at www.sciencedirect.com

Journal of Molecular Biology

journal homepage: http://ees.elsevier.com.jmb

Structure-Guided Activity Restoration of the Silkworm Glutathione Transferase Omega GSTO3-3

Bao-Yu Chen[1]†, Xiao-Xiao Ma[1]†, Peng-Chao Guo[1], Xiang Tan[2], Wei-Fang Li[1], Jie-Pin Yang[1], Nan-Nan Zhang[1], Yuxing Chen[1], Qingyou Xia[2] and Cong-Zhao Zhou[1]*

[1]*School of Life Sciences and Hefei National Laboratory for Physical Sciences at the Microscale, University of Science and Technology of China, Hefei, Anhui 230027, People's Republic of China*
[2]*Key Sericultural Laboratory of Agricultural Ministry, Institute of Sericulture and Systems Biology, Southwest University, Chongqing 400716, China*

Received 2 April 2011; received in revised form 11 July 2011; accepted 12 July 2011
Available online 21 July 2011

Edited by R. Huber

Keywords:
Bombyx mori;
glutathione transferase Omega;
crystal structure;
site-directed mutagenesis;
enzymatic activity

Glutathione transferases (GSTs) are ubiquitous detoxification enzymes that conjugate hydrophobic xenobiotics with reduced glutathione. The silkworm *Bombyx mori* encodes four isoforms of GST Omega (GSTO), featured with a catalytic cysteine, except that bmGSTO3-3 has an asparagine substitution of this catalytic residue. Here, we determined the 2.20-Å crystal structure of bmGSTO3-3, which shares a typical GST overall structure. However, the extended C-terminal segment that exists in all the four bmGSTOs occupies the G-site of bmGSTO3-3 and makes it unworkable, as shown by the activity assays. Upon mutation of Asn29 to Cys and truncation of the C-terminal segment, the *in vitro* GST activity of bmGSTO3-3 could be restored. These findings provided structural insights into the activity regulation of GSTOs.

Introduction

Glutathione transferases (GSTs; EC 2.5.1.18) are widely distributed enzymes that are related to various functions, such as detoxification and antioxidation.[1] The enzymatic detoxification of xenobiotics has been classified into three distinct phases that act in a tightly integrated manner. GSTs are phase II detoxification enzymes and have a crucial role in a series of complex detoxification strategies.[2] These enzymes catalyze nucleophilic attack of the reduced glutathione (GSH) on hydrophobic compounds such as pyrethroid, organophosphate, arene oxides, quinones, and α,β-unsaturated carbonyl compounds.[1,3,4] Besides the GST activity, some GSTs have been found to play an important role in binding toxic compounds to fight against oxidative stress.[5]

Based on sequence alignments, cytosolic GSTs are grouped into eight main strain classes: α, π, μ, θ, κ, ζ, ω, and σ in mammals. In addition, several new classes have been found by studies of nonmammalian species, such as the φ-class and τ-class in plants, the δ-class in insects, and the β-class in bacteria.[2,6] Meanwhile, according to catalytic residues of the active site, all cytosolic GSTs of known structure can be classified into three typical catalytic types: tyrosine, serine or cysteine,[2,3] and an atypical type.[7] Site-directed mutagenesis has proved that these catalytic residues are essential for the reaction.[2,8]

*Corresponding author. E-mail address: zcz@ustc.edu.cn.
† B.-Y.C. and X.-X.M. contributed equally to this work.
Abbreviations used: GST, glutathione transferase; GSH, reduced glutathione; CDNB, 1-chloro-2,4-dinitrobenzene; GSTO, GST Omega; PDB, Protein Data Bank.

It has been reported that GSTs in multiple isoforms at various developmental stages are expressed at a high level.[2,9,10] The silkworm *Bombyx mori* genome encodes 23 putative cytosolic GSTs.[11] They not only cover all six classes (δ, ε, σ, θ, ζ, and ω) found in other insects[12] but also contain two classes that cannot be assigned into the known classes.[11] There are four isoforms of GST Omega (GSTO) in the silkworm, termed bmGSTO1-1 to bmGSTO4-4. Three of them (bmGSTO1-1, bmGSTO2-2, and bmGSTO4-4) share a high level of sequence identity (>40%), whereas bmGSTO3-3 shows a relatively low level of identity (29%) with the former three. In contrast, bmGSTO3-3 shares an identity from 31.8% to 39.3% with other insect GSTOs.[11]

Multiple-sequence alignment indicated that GSTOs have an N-terminal and a C-terminal long segment distinguished from members of other GST classes. Its catalytic cysteine can form a disulfide bond with GSH in the active site.[2,13] Although GSTs have been extensively studied, human GSTO1-1 [hGSTO1-1; Protein Data Bank (PDB) code: 1EEM] is the only one GSTO of known structure.[13] Here, we determined the crystal structure of bmGSTO3-3 at 2.20 Å resolution. It has a classical GST fold that contains an N-terminal thioredoxin-like domain and a C-terminal all-α domain. Enzymatic assays show that bmGSTO3-3 has a very low activity toward the standard GST substrate 1-chloro-2,4-dinitrobenzene (CDNB). However, upon mutation of Asn29 to Cys and truncation of the C-terminal segment, the *in vitro* activity of bmGSTO3-3 could be restored. These findings provided the first structural insights into the activation of all GSTOs with an extended C-terminal segment.

Results and Discussion

Overall structure of bmGSTO3-3

Although each asymmetric unit of the crystal contains four chains of bmGSTO3-3, the size-exclusion chromatography confirmed that bmGSTO3-3 exists as a dimer in solution (Fig. 1a). The dimeric interface is 1930 Å^2, similar to that (1960 Å^2) of hGSTO1-1.[13] The inter-subunit interactions are mainly mediated by hydrophobic residues on helices α3 and α4. Each subunit of bmGSTO3-3 adopts a typical GST fold, similar to the reported GST structures, which contains a thioredoxin-like N-terminal domain and an all-α C-terminal domain (Fig. 1b and c). Distinct from GSTs of other classes, bmGSTO3-3 has extra loops at both termini as found in hGSTO1-1.[13]

The four chains in an asymmetric unit share an almost identical overall structure, except for the conformations around the C-terminus. The C-termini of three chains (A, B, and D) present as a flexible loop that occupies the conserved GSH binding site (G-site) (Fig. 1b), whereas that of chain C adopts a helix conformation to form an extended helix α10 (Fig. 1c).

The G-site and H-site

The overall structure of bmGSTO3-3 could be well superimposed to that of hGSTO1-1, except for the C-terminal segments, which adopt different conformations (Fig. 2a). Moreover, the catalytic cysteine is replaced by an asparagine in bmGSTO3-3 (Fig. 2b), even though other residues around the G-site of bmGSTO3-3 are highly conserved. The cysteine in the G-site of mammalian GSTOs is generally accepted to form a mixed disulfide bond with GSH.[2,13,14] We tried co-crystallization of bmGSTO3-3 with GSH but did not succeed. One reason is that the C-terminal loop occupies the G-site (Fig. 2a), leading to the inaccessibility of GSH. In contrast to the conserved G-site, the substrate binding site (H-site) is composed of variable hydrophobic residues, which could facilitate the binding of diverse hydrophobic substrates.

Recovery of the GST activity of bmGSTO3-3

The yeast *Saccharomyces cerevisiae* Ure2 contains a C-terminal globular domain that shows similarity to

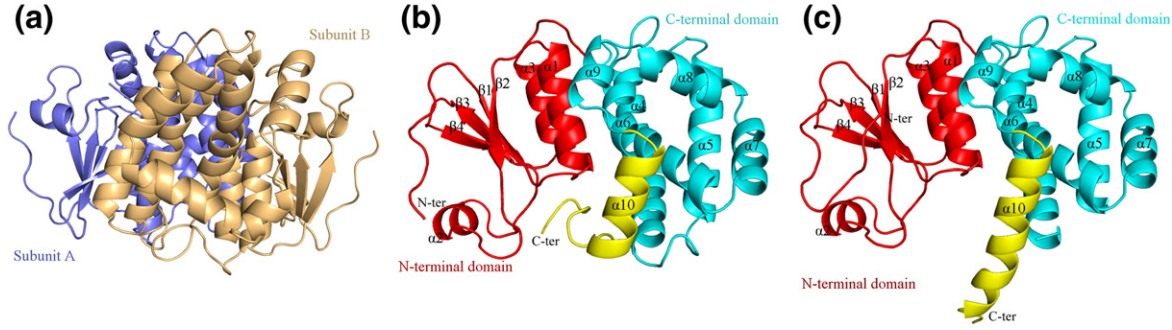

Fig. 1. Overall structure of bmGSTO3-3. (a) Schematic representation of the bmGSTO3-3 homodimer. The bmGSTO3-3 monomers of (b) chain A and (c) chain C, with the two domains in cyan and red, respectively. The C-terminal segments of chain A and chain C have different conformations, as colored yellow.

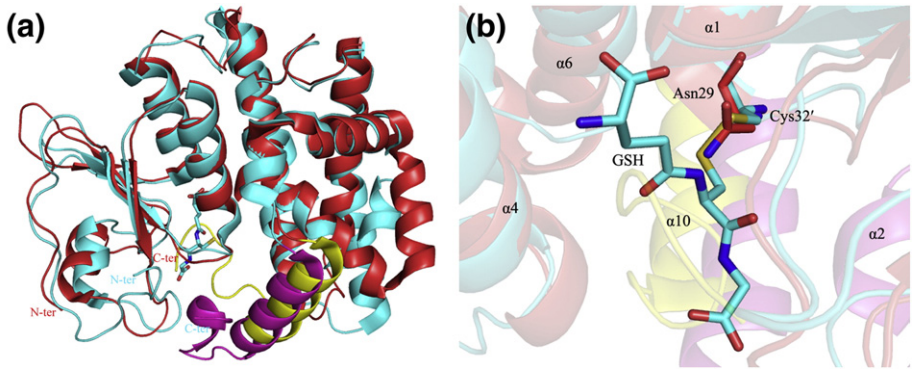

Fig. 2. Superposition of bmGSTO3-3 against hGSTO1-1. (a) The core structures of bmGSTO3-3 and hGSTO1-1 are colored red and cyan, respectively, whereas the C-terminal segments are colored yellow and magenta, respectively. (b) Asn29 in bmGSTO3-3 is superimposed to Cys32′ in hGSTO1-1. The GSH is covalently linked to the catalytic cysteine of hGSTO1-1.

GSTs in both sequence and structure.[15] However, Ure2 showed no detectable GST activity toward the standard substrate CDNB, which might be due to the absence of a catalytic residue. After a single mutation of Ala or Asn around the N-terminus of helix α1, the authors restored the GST activity of Ure2.[15] Structural analysis in combination with multiple-sequence alignment (Fig. 3) indicated that bmGSTO3-3 had neither a catalytic residue (Tyr, Ser, or Cys) nor a special water molecule around.[7] *In vitro* GST activity assays revealed that bmGSTO3-3 could not facilitate the conjugation of GSH to CDNB. One reason is that the catalytic cysteine is replaced by an asparagine in bmGSTO3-3; thus, the GSH could not be activated. The other reason is that the C-terminal segment occupies the G-site; thus, no GSH could enter.

In order to check these two possible reasons, we first mutated Asn29 to Cys for enzymatic assays. Out of our expectation, the activity of the N29C mutant is nearly undetectable as the wild-type bmGSTO3-3 (Fig. 4a). Meanwhile, we truncated the 12 residues of the C-terminal loop and detected the activity of bmGSTO3-3ΔC12, which remains inactive (Fig. 4a). Further structural analysis revealed that the side chains of residues on helix α10 are too close to the G-site and probably could also impede catalysis. Thus, we deleted 10 more residues of the C-terminus and measured the activity of bmGSTO3-3ΔC22. However, the truncation of 22 residues from the C-terminus only slightly elevates the activity (Fig. 4a). We proposed that, after truncation, the G-site of bmGSTO3-3 was exposed and accessible to GSH, but Asn29 seems not to be as efficient as Cys, probably due to its stronger stereo-hindrance or incapability to stabilize the thiolate anion.

Therefore, we combined Asn29Cys mutation and C-terminus deletion and found that the GST activity of bmGSTO3-3ΔC22N29C was greatly improved (Fig. 4a). The K_m value of bmGSTO3-3ΔC22N29C toward CDNB is 1.01 ± 0.10 mM, V_{max} is 0.64 ± 0.02 μmol/mg/min, and k_{cat}/K_m is 0.297 ± 0.009 mM^{-1} s^{-1} (Fig. 4b). All protein samples were quality controlled by circular dichroism (CD) spectroscopy, indicating that the three mutations did not introduce significant changes to the protein structure (Supplementary Fig. S1). Moreover, the V_{max} value is comparable to that of typical GSTOs (*Neanthes succinea* GSTO, 3.34 ± 0.18 μmol/mg/min[16]; hGSTO1-1, 0.18 ± 0.006 μmol/mg/min[13]). Even though the kinetic constants of other GSTOs are not available, the K_m value of bmGSTO3-3ΔC22N29C toward CDNB is similar to that of most GSTs from other classes, such as *Ochrobactrum anthropi* GST[17] (3.09 ± 0.22 mM, β-class), *Anopheles dirus* GSTD4[18] (0.50 ± 0.02 mM, δ-class), human GSTA1-1[19] (0.33 ± 0.06 mM, α-class), and human GSTP1-1[20] (0.56 ± 0.05 mM, π-class), whereas the k_{cat}/K_m value for bmGSTO3-3ΔC22N29C is 10- to 1000-fold lower than these GSTs (*O. anthropi* GST,[17] 5.33 mM^{-1} s^{-1}; *A. dirus* GSTD4,[18] 51.84 mM^{-1} s^{-1}; human GSTA1-1,[19] 103.5 ± 28.3 mM^{-1} s^{-1}; human GSTP1-1,[20] 214 ± 1.4 mM^{-1} s^{-1}). Our results are also in agreement with the previous reports that GSTOs have a poor activity toward the common GST substrate CDNB.[21]

To further validate the necessity of Cys29, we modified Cys29 with a Cys-reactive chemical, iodoacetamide, which could block the reduced SH group by alkylation. Results showed that the activity was greatly decreased upon the modification of Cys29 (Fig. 4a). Moreover, we used intrinsic fluorescence spectroscopy to assess the substrate-binding ability of the H-site in wild-type protein and mutants. Results showed that both samples exhibit a similar affinity toward CDNB (K_d = 111.03 ± 8.12 μM for the wild type and K_d = 103.03 ± 8.07 μM for bmGSTO3-3ΔC22N29C; Fig. 5a and b), but the activity of either the wild type or the N29C mutant was too low to be detectable, while the activity of bmGSTO3-3ΔC22N29C was greatly improved.

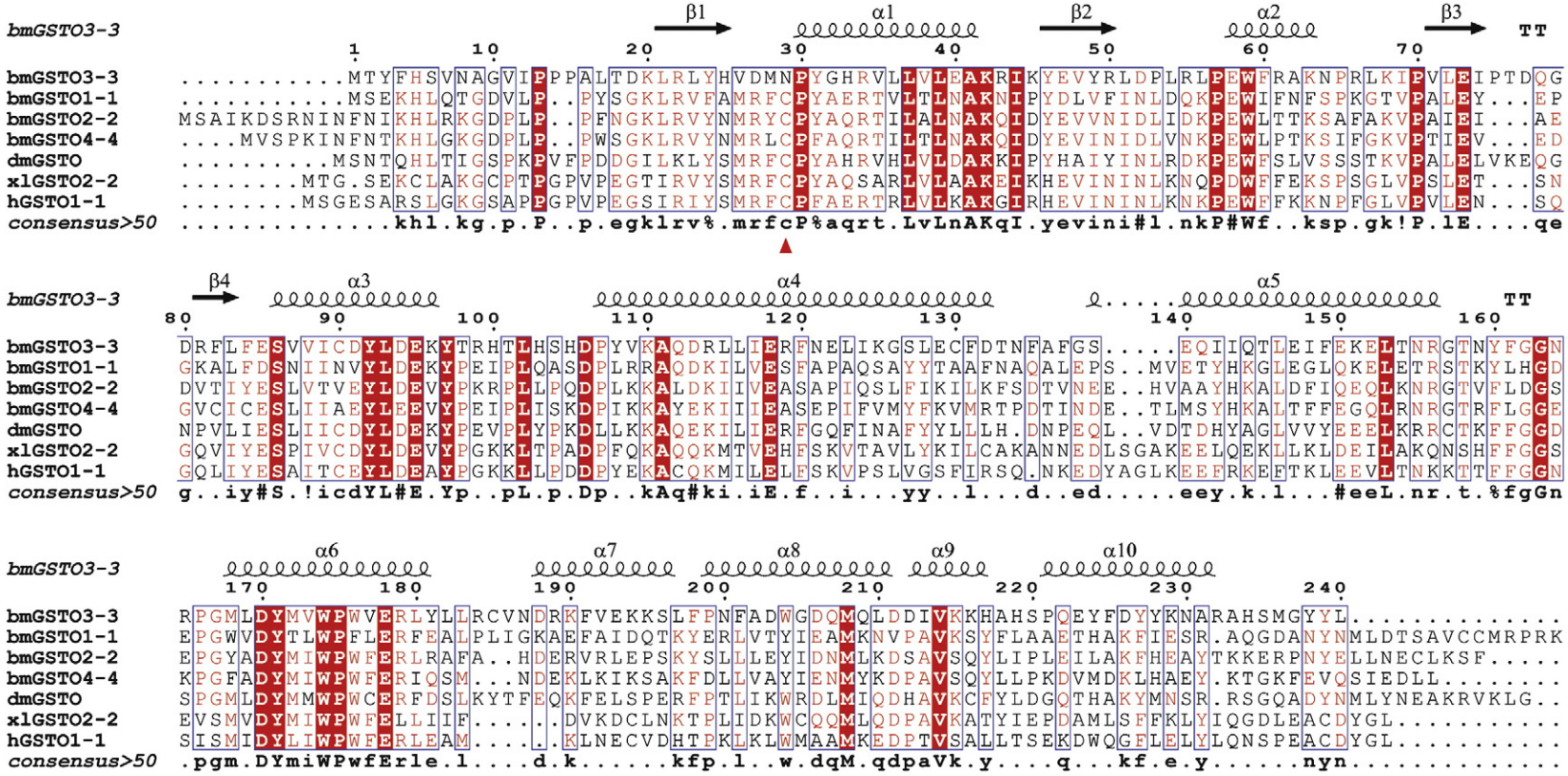

Fig. 3. The multiple-sequence alignment of GSTOs. The sequences include bmGSTO1-1 (Q2F689), bmGSTO2-2 (Q2I0J6), bmGSTO3-3 (Q1HPV9), bmGSTO4-4 (B0LKP6), *Drosophila* dmGSTO (D1KS75), *Xenopus* xlGSTO2-2 (A8E5X8), and hOmega1-1 (P78417). The essential residue of GSH binding site is marked in red triangle.

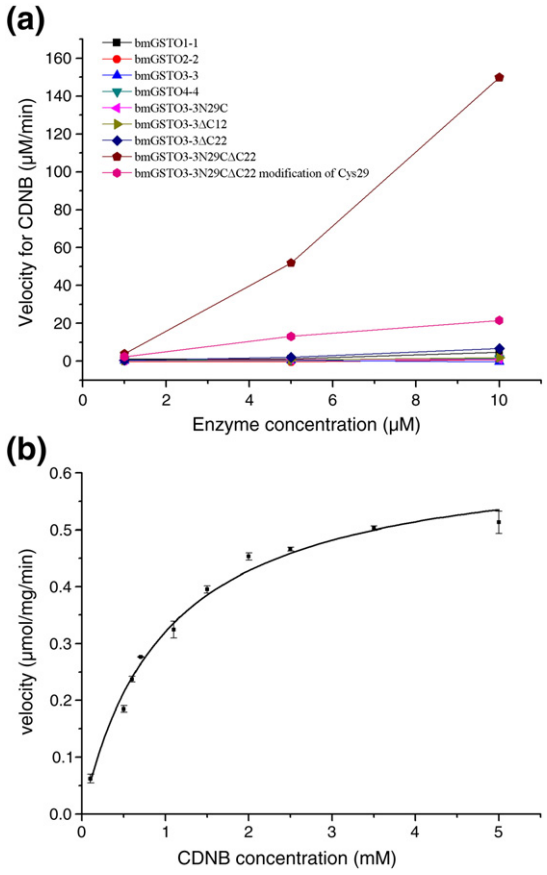

Fig. 4. The enzymatic activity of bmGSTO3-3. (a) The relative activity of the wild-type bmGSTO3-3, four bmGSTO3-3 mutants, and the other three bmGSTOs. (b) The reaction kinetics of bmGSTO3-3N29CΔC22.

These results demonstrated that the inactivation of the wild type and the N29C mutant is due to the unavailability of an active G-site to GSH but not to the dysfunction of the H-site. Moreover, the great improvement in activity of bmGSTO3-3ΔC22N29C demonstrates that both the catalytic cysteine and an accessible G-site are indispensable factors for catalysis.

Putative functions of *B. mori* GSTOs

We further measured the activity of the other three bmGSTOs (bmGSTO1-1, bmGSTO2-2, and bmGSTO4-4) with the same method mentioned above. The results showed that the activity of these GSTOs were similar to that of bmGSTO3-3N29C, which is nearly undetectable (Fig. 4a). Moreover, multiple-sequence alignment indicated that all the four GSTOs have a long C-terminal segment, which might form an α-helix followed by a loop as predicted by PSIPRED server.[22] Thus, it is possible that the C-terminal segment of bmGSTOs leads to their low activity toward CDNB. The C-terminal segment of other bmGSTOs probably could also occupy the G-site and prevent the binding of GSH, as observed in the structure of bmGSTO3-3. After the removal of the C-terminal segment, the GST activity of these GSTOs could be restored as well. This property implies that bmGSTOs may have two possible functions. One is that the C-terminal segments of the bmGSTOs are very rigid *in vivo*; thus, these enzymes could not bind GSH and lose their conjugation activities. However, the functional H-sites enable them to bind or/and transfer the toxic compounds, as reported previously for other GSTs.[5,23,24] The other possibility is that bmGSTOs still maintain their GST activity, but some cofactors are needed to shift the C-terminal segments away from the G-site. However, more investigations are needed to reach a convincing explanation on their actual roles *in vivo*.

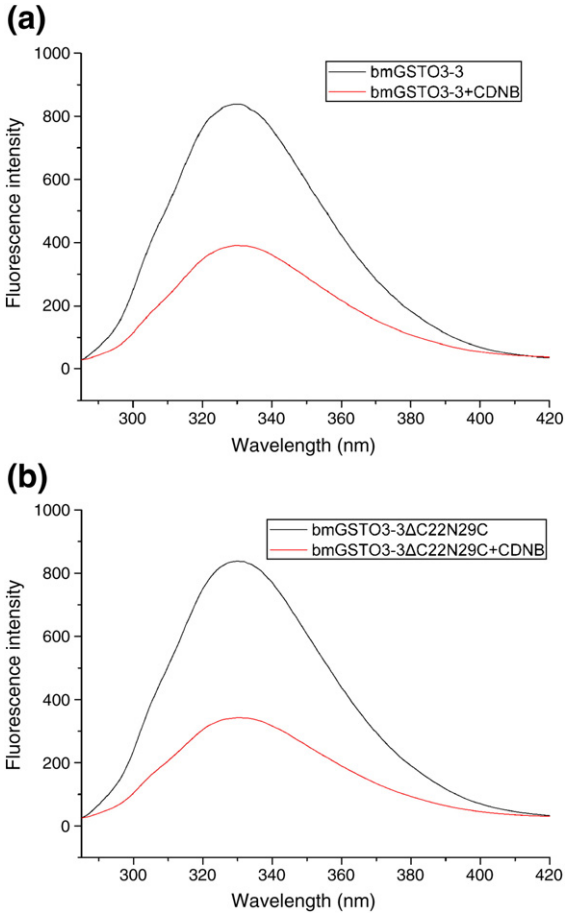

Fig. 5. Intrinsic fluorescence assays. Fluorescence spectra of (a) the wild-type bmGSTO3-3 and (b) bmGSTO3-3N29CΔC22. The black and red lines represent the spectra of the apo-form and the CDNB-bound form, respectively.

Materials and Methods

Construction, expression, and purification of bmGSTO3-3

The coding region of bmGSTO3-3 was amplified and cloned into a pET28a-derived expression vector with a hexa-histidine (6× His) tag just after the start codon. The recombinant plasmid was transformed into *Escherichia coli* BL21 (DE3) strain and cultured with 2× YT medium (16 g of tryptone, 10 g of yeast extract, and 5 g of NaCl per liter). When the cells were grown to an $OD_{600\ nm}$ of 0.6–0.8 at 37 °C, expression was induced by adding 0.2 mM isopropyl-β-D-thiogalactopyranoside, and the cells continued growing for another 20 h at 16 °C. Cells were collected by centrifugation and resuspended in lysis buffer [20 mM Tris–HCl (pH 8.5), 100 mM NaCl, and 14 mM β-mercaptoethanol]. After freezing–thawing, sonication, and centrifugation, the supernatant was collected and loaded onto a Ni-NTA column (Amersham Biosciences) equilibrated with lysis buffer [20 mM Tris–HCl (pH 8.5), 100 mM NaCl, and 14 mM β-mercaptoethanol]. The target protein was eluted with a linear gradient of imidazole from 20 to 300 mM and further purified with a HiLoad 16/60 Superdex 75 column (GE Healthcare) equilibrated with 20 mM Tris–HCl (pH 8.5), 100 mM NaCl, 2 mM ethylenediaminetetraacetic acid, 5% glycerol, and 14 mM β-mercaptoethanol. The protein for enzymatic assay is purified in a buffer containing 20 mM Tris–HCl (pH 8.5) and 100 mM NaCl and concentrated to 3 mg/ml. The purity was checked by SDS-PAGE.

Crystallization, data collection, and processing

Crystallization was carried out at 289 K using the hanging-drop vapor-diffusion techniques. Drops were prepared by mixing 2 μl protein sample containing 20 mM dithiothreitol with 1 μl reservoir solution [0.2 M $MgCl_2$, 0.1 M Tris–HCl (pH 8.5), 25% polyethylene glycol 3350, and 10% glycerol]. The crystals appeared in 2 days. After the transfer into the cryoprotectant (the reservoir solution supplemented with 25% glycerol), the crystals were flash frozen with liquid nitrogen. The X-ray diffraction data were collected with a MX-225 CCD using the BL17U beamline at the Shanghai Synchrotron Radiation Facility. The data were processed with the program HKL2000.[25]

Structure determination and refinement

The structure of bmGSTO3-3 was determined by molecular replacement with Phaser[26] in CCP4[27] using hGSTO1-1 (PDB code: 1EEM)[13] as a search model. Refinement was performed with REFMAC[28] and Coot.[29] The overall assessment of model quality was performed using MolProbity.[30] Crystallographic parameters of the structure are listed in Table 1. All structure figures were prepared with PyMOL.[31]

Enzymatic assay

The activities of bmGSTO3-3, bmGSTO3-3ΔC12, bmGSTO3-3ΔC22, and other mutants toward CDNB were measured at 340 nm ($\varepsilon_{340} = 9.6\ mM^{-1}\ cm^{-1}$) according to previous reports.[32] CDNB is the standard substrate for GST enzymatic assay.[33,34] The activity toward CDNB was performed with 0.1 M potassium phosphate (pH 6.5), 1 mM GSH, 1 mM CDNB, and 1–10 μM enzyme. Measurements were carried out with a DU-800 spectrophotometer (Beckman Coulter, Fullerton, CA, USA). The reaction was monitored for 180 s with an interval of 15 s. The K_m and V_{max} of bmGSTO3-3ΔC22N29C were measured in the buffer of 0.1 M potassium phosphate (pH 6.5), 1 mM GSH, 0.1–5 mM CDNB, and 3 μM enzyme. The reaction was monitored for 180 s with an interval of 12 s.

Table 1. Data collection and structure refinement

Data collection	
Wavelength (Å)	0.9790
Space group	$C222_1$
Unit cell (Å, °)	$a=108.54$, $b=139.03$, $c=128.82$ $\alpha=\beta=\gamma=90$
Molecules per asymmetric unit	4
Resolution range (Å)[a]	50.00–2.20 (2.28–2.20)
Unique reflections	49,572 (4858)
Completeness (%)	99.8 (99.2)
$\langle I/\sigma(I)\rangle$	21.3 (3.4)
R_{merge}[b] (%)	8.7 (47.7)
Average redundancy	7.0
Refinement statistics	
Resolution range (Å)	50.00–2.20 (2.26–2.20)
R-factor[c]/R_{free}[d] (%)	21.5/26.3
Number of protein atoms	7859
Number of water atoms	357
RMSD[e] bond lengths (Å)	0.008
RMSD bond angles (°)	1.052
Mean *B*-factors (Å^2)	32.2
Ramachandran plot[f] (%)	
Most favored	97.8
Additional allowed	1.8
PDB entry	3RBT

[a] The values in parentheses refer to statistics in the highest bin.
[b] $R_{merge} = \sum_{hkl}\sum_i |I_i(hkl) - \langle I(hkl)\rangle| / \sum_{hkl}\sum_i I_i(hkl)$, where $I_i(hkl)$ is the intensity of an observation, and $\langle I(hkl)\rangle$ is the mean value for its unique reflection. Summations are the overall reflections.
[c] *R*-factor $= \sum_h |F_o(h) - F_c(h)| / \sum_h F_o(h)$, where F_o and F_c are the observed and calculated structure factor amplitudes, respectively.
[d] R_{free} was calculated with 5% of the data excluded from the refinement.
[e] RMSD from ideal values.
[f] Categories were defined by MolProbity.

CD assays

CD spectra were performed with a Jasco J-810 system (Jasco Instruments, Tokyo, Japan). Spectra of the wild-type bmGSTO3-3 and three mutants were recorded from 195 to 260 nm with a protein concentration of 0.1 mg/ml in 100 mM potassium phosphate (pH 6.5). The curves were fitted using the Jasco J-810 accessory secondary structure analysis program to estimate the protein secondary structures.[35]

Modification of Cys29

The protein sample of bmGSTO3-3ΔC22N29C (20 μM) was mixed with iodoacetamide (5 mM) in a final volume

of 5 ml. Labeling of bmGSTO3-3ΔC22N29C was performed in 100 mM potassium phosphate buffer, pH 6.5. Incubation was carried out on ice for 2 h. After incubation, the mixture was applied to a Sephadex G-25F column equilibrated with 100 mM potassium phosphate buffer, pH 6.5, to remove the extra iodoacetamide.[36]

Intrinsic fluorescence spectroscopy

Protein intrinsic fluorescence spectra were monitored at a wavelength from 285 to 420 nm using an RF-5301PC spectrofluorophotometer (Shimadzu). Considering the higher content of tyrosine compared to tryptophan residues in bmGSTO3-3, we used an excitation wavelength at 275 nm to measure the intrinsic fluorescence of tyrosine side chains. Before measurement, a quartz cuvette containing 250 μl protein sample (1 μM) was incubated with the substrate CDNB at various concentrations for 10 min at 25 °C. CDNB was dissolved in absolute alcohol (the final concentration of alcohol in assay was 2%).

Accession numbers

The coordinates and the structure factors of bmGSTO3-3 have been deposited in the Research Collaboratory for Structural Bioinformatics PDB‡ under the accession code 3RBT.

Supplementary materials related to this article can be found online at doi:10.1016/j.jmb.2011.07.019

Acknowledgements

We appreciate the help of the staff at the Shanghai Synchrotron Radiation Facility. This work was supported by the National Natural Science Foundation of China (Program 30870490) and the Ministry of Science and Technology of China (Projects 2005CB121002 and 2006AA10A119).

References

1. Hayes, J. D., Flanagan, J. U. & Jowsey, I. R. (2005). Glutathione transferases. *Annu. Rev. Pharmacol. Toxicol.* **45**, 51–88.
2. Sheehan, D., Meade, G., Foley, V. M. & Dowd, C. A. (2001). Structure, function and evolution of glutathione transferases: implications for classification of non-mammalian members of an ancient enzyme superfamily. *Biochem. J.* **360**, 1–16.
3. Armstrong, R. N. (1997). Structure, catalytic mechanism, and evolution of the glutathione transferases. *Chem. Res. Toxicol.* **10**, 2–18.
4. Yu, S. J. (1992). Detection and biochemical characterization of insecticide resistance in fall armyworm (Lepidoptera: Noctuidae). *J. Econ. Entomol.* **85**, 675–682.
5. Hayes, J. D. & Pulford, D. J. (1995). The glutathione *S*-transferase supergene family: regulation of GST and the contribution of the isoenzymes to cancer chemoprotection and drug resistance. *Crit. Rev. Biochem. Mol. Biol.* **30**, 445–600.
6. Allocati, N., Federici, L., Masulli, M. & Di Ilio, C. (2009). Glutathione transferases in bacteria. *FEBS J.* **276**, 58–75.
7. Ma, X. X., Jiang, Y. L., He, Y. X., Bao, R., Chen, Y. & Zhou, C. Z. (2009). Structures of yeast glutathione-*S*-transferase Gtt2 reveal a new catalytic type of GST family. *EMBO Rep.* **10**, 1320–1326.
8. Casalone, E., Allocati, N., Ceccarelli, I., Masulli, M., Rossjohn, J., Parker, M. W. & Di Ilio, C. (1998). Site-directed mutagenesis of the *Proteus mirabilis* glutathione transferase B1-1 G-site. *FEBS Lett.* **423**, 122–124.
9. Yu, S. J. (1996). Insect glutathione *S*-transferases. *Zool. Stud.* **35**, 9–19.
10. Zhou, Z. H. & Syvanen, M. (1997). A complex glutathione transferase gene family in the housefly *Musca domestica*. *Mol. Gen. Genet.* **256**, 187–194.
11. Yu, Q., Lu, C., Li, B., Fang, S., Zuo, W., Dai, F. *et al.* (2008). Identification, genomic organization and expression pattern of glutathione *S*-transferase in the silkworm, *Bombyx mori*. *Insect Biochem. Mol. Biol.* **38**, 1158–1164.
12. Ding, Y., Ortelli, F., Rossiter, L. C., Hemingway, J. & Ranson, H. (2003). The *Anopheles gambiae* glutathione transferase supergene family: annotation, phylogeny and expression profiles. *BMC Genomics*, **4**, 35.
13. Board, P. G., Coggan, M., Chelvanayagam, G., Easteal, S., Jermiin, L. S., Schulte, G. K. *et al.* (2000). Identification, characterization, and crystal structure of the Omega class glutathione transferases. *J. Biol. Chem.* **275**, 24798–24806.
14. Rossjohn, J., Polekhina, G., Feil, S. C., Allocati, N., Masulli, M., De Illio, C. & Parker, M. W. (1998). A mixed disulfide bond in bacterial glutathione transferase: functional and evolutionary implications. *Structure*, **6**, 721–734.
15. Zhang, Z. R., Bai, M., Wang, X. Y., Zhou, J. M. & Perrett, S. (2008). "Restoration" of glutathione transferase activity by single-site mutation of the yeast prion protein Ure2. *J. Mol. Biol.* **384**, 641–651.
16. Rhee, J. S., Lee, Y. M., Hwang, D. S., Lee, K. W., Kim, I. C., Shin, K. H. *et al.* (2007). Molecular cloning and characterization of omega class glutathione *S*-transferase (GST-O) from the polychaete *Neanthes succinea*: biochemical comparison with theta class glutathione *S*-transferase (GST-T). *Comp. Biochem. Physiol., Toxicol. Pharmacol.* **146**, 471–477.
17. Allocati, N., Federici, L., Masulli, M., Favaloro, B. & Di Ilio, C. (2008). Cysteine 10 is critical for the activity of *Ochrobactrum anthropi* glutathione transferase and its mutation to alanine causes the preferential binding of glutathione to the H-site. *Proteins*, **71**, 16–23.
18. Vararattanavech, A. & Ketterman, A. J. (2007). A functionally conserved basic residue in glutathione transferases interacts with the glycine moiety of glutathione and is pivotal for enzyme catalysis. *Biochem. J.* **406**, 247–256.

‡ http://www.rcsb.org

19. Nathaniel, C., Wallace, L. A., Burke, J. & Dirr, H. W. (2003). The role of an evolutionarily conserved *cis*-proline in the thioredoxin-like domain of human class Alpha glutathione transferase A1-1. *Biochem. J.* **372**, 241–246.
20. Hegazy, U. M., Mannervik, B. & Stenberg, G. (2004). Functional role of the lock and key motif at the subunit interface of glutathione transferase P1-1. *J. Biol. Chem.* **279**, 9586–9596.
21. Whitbread, A. K., Tetlow, N., Eyre, H. J., Sutherland, G. R. & Board, P. G. (2003). Characterization of the human Omega class glutathione transferase genes and associated polymorphisms. *Pharmacogenetics*, **13**, 131–144.
22. Jones, D. T. (1999). Protein secondary structure prediction based on position-specific scoring matrices. *J. Mol. Biol.* **292**, 195–202.
23. Ishigaki, S., Abramovitz, M. & Listowsky, I. (1989). Glutathione-*S*-transferases are major cytosolic thyroid hormone binding proteins. *Arch. Biochem. Biophys.* **273**, 265–272.
24. Tipping, E., Ketterer, B. & Koskelo, P. (1978). The binding of porphyrins by ligandin. *Biochem. J.* **169**, 509–516.
25. Otwinowski, Z. & Minor, W. (1997). Processing of X-ray diffraction data collected in oscillation mode. *Macromol. Crystallogr., Part A, 1997*, **276**, 307–326.
26. McCoy, A. J. (2007). Solving structures of protein complexes by molecular replacement with Phaser. *Acta Crystallogr., Sect. D: Biol. Crystallogr.* **63**, 32–41.
27. Bailey, S. (1994). The CCP4 suite: programs for protein crystallography. *Acta Crystallogr., Sect. D: Biol. Crystallogr.* **50**, 760–763.
28. Murshudov, G. N., Vagin, A. A. & Dodson, E. J. (1997). Refinement of macromolecular structures by the maximum-likelihood method. *Acta Crystallogr., Sect. D: Biol. Crystallogr.* **53**, 240–255.
29. Emsley, P. & Cowtan, K. (2004). Coot: model-building tools for molecular graphics. *Acta Crystallogr., Sect. D: Biol. Crystallogr.* **60**, 2126–2132.
30. Lovell, S. C., Davis, I. W., Arendall, W. B., III, de Bakker, P. I., Word, J. M., Prisant, M. G. *et al.* (2003). Structure validation by C^{α} geometry: ϕ,ψ and C^{β} deviation. *Proteins*, **50**, 437–450.
31. DeLano, W. (2002). *The PyMOL Molecular Graphics System.* DeLano Scientific, San Carlos, CA.
32. Habig, W. H. & Jakoby, W. B. (1981). Assays for differentiation of glutathione *S*-transferases. *Methods Enzymol.* **77**, 398–405.
33. Kim, J., Suh, H., Kim, S., Kim, K., Ahn, C. & Yim, J. (2006). Identification and characteristics of the structural gene for the *Drosophila* eye colour mutant *sepia*, encoding PDA synthase, a member of the Omega class glutathione *S*-transferases. *Biochem. J.* **398**, 451–460.
34. Board, P. G. & Anders, M. W. (2007). Glutathione transferase omega 1 catalyzes the reduction of *S*-(phenacyl)glutathiones to acetophenones. *Chem. Res. Toxicol.* **20**, 149–154.
35. Yang, J. T., Wu, C. S. & Martinez, H. M. (1986). Calculation of protein conformation from circular dichroism. *Methods Enzymol.* **130**, 208–269.
36. Chernogolov, A., Usanov, S., Kraft, R. & Schwartz, D. (1994). Selective chemical modification of Cys^{264} with diiodofluorescein iodacetamide as a tool to study the membrane topology of cytochrome P450scc (CYP11A1). *FEBS Lett.* **340**, 83–88.